Contents list available at CBIORE journal website

International Journal of Renewable Energy Development

Journal homepage: https://ijred.cbiore.id

Research Article

Enhancement of aerodynamic performance of H-Darrieus rotor using wraparound fairing system: A 2D CFD study

Douha Boulla[a*], Saïf ed-Dîn Fertahi[a], Maryam Bernatchou[b], Abderrahim Samaouali[a], Meryeme Ajani[a], Chaimae Boussaq[a]

[a] *Physics Department, Thermodynamics and Energy Research Team, Energy Research Center, Faculty of Science, Mohammed V University in Rabat, 4 Avenue Ibn Batouta, BP 1014, Rabat 10000, Morocco*

[b] *Physics Department, Team of Modeling and Simulation in Mechanics and Energetics (MSME), Faculty of Sciences, Mohammed V University in Rabat, 4 Avenue Ibn Batouta, Rabat, B.P. 1014, Morocco*

Abstract. The aim of this article is to improve the aerodynamic performance of a three-bladed vertical axis H-Darrieus wind turbine, which is equipped with different types of fairings. To this end, a 2D CFD simulation combined with calculations based on the resolution of the Steady Reynolds-Averaged Navier-Stokes equations (RANS) and the SST $k-\omega$ turbulence model was used. In addition, the multiple reference frame (MRF) method was applied for the simulation. The simulation results show that the power coefficient (C_P) reaches maximum values equal to 0.561, 0.580 and 0.607 for the NACA2412, Eppler 423 and DAE-11 profiles respectively, for a chord length C = 3 and a tip speed ratio (TSR) equal to 2.5. Then, the torque coefficient (C_m) reaches the highest value of C_m = 0.354 at α = 20° for the DAE-11 fairing, which means that this profile performs better, particularly at higher angles of attack. These results confirm that the DAE-11 fairing surpassed the Eppler 423 and NACA2412 profiles. Unstable vortex field formation has been observed between the turbine and the fairing, at the leading and trailing edges, for both low and high fairing chord lengths. This phenomenon can increase torque and disrupt flow direction at low velocity. On the other hand, when the chord length reaches a medium value, a more stable flow zone appears. It can therefore be concluded that the addition of a fairing to the H-Darrieus rotor with a suitable chord length improves the turbine aerodynamic performance, particularly in terms of flow stabilization and reduction of the stagnation zone.

Keywords: CFD, H-Darrieus, MRF, power coefficient, torque coefficient, fairing, performance assessment, NACA0018

Received: 3rd June 2025; Revised: 29th July 2025; Accepted: 15th August 2025; Available online: 25th August 2025

1. Introduction

The significant increase in demand for electricity over the current decade presents a substantial issue for the energy sector, which must meet these high requirements. However, renewable energies play an important role in economic expansion and sustainable development. In recent years, significant initiatives have been implemented to accelerate the adoption of renewable energy sources, which are environmentally friendly and contribute to mitigation of climate change by reducing greenhouse gas emissions (NEA Releases 2002). Moreover, particular attention has also been granted to wind power technologies, which occupy a strategic position in the energy transition, endowing with high development potential and significant economic and ecological advantages. These winds powered turbines consist of two categories: horizontal axis wind turbines (HAWTs) and vertical axis wind turbines (VAWTs). In the case of (VAWTs), it could be subdivided into two types: Savonius and Darrieus. Savonius vertical axis wind turbines, due to their simple design, are adapted to low power applications, while Darrieus vertical axis wind turbines are more efficient and more widely used for large scale energy production (Hau 2006).

In the literature, number of studies have focused on improving the aerodynamic performance of the H-Darrieus turbine. Among these works, we cite (Chowdhury *et al.* 2022), which have concentrated on the impacts and technical aspects of traditional wind farms, while examining recent developments within the scientific community to identify potential areas of research for technical performance and policy evolution. Pedram (Ghiasi *et al.* 2023*)* examined the performance of the Darrieus vertical axis wind turbine, investigating the effect of chord length, blade thickness and angle of attack at different tip speed ratio (TSR). Their results show that increasing chord length from 0.1 to 0.2 m improves drag-lift performance. (Gebreel *et al.* 2017*)* presented an intelligent control using a multilayer perceptron artificial neural network (MLP-ANN) with variable pitch angle to improve the performance of H-Darrieus VAWTs for different values of tip speed ratio (TSR), using ANSYS Fluent software through 2D CFD simulation.

Mandar Tabib *et al.* (2017*)* carried out a comparison of the three methods, namely Actuator Line Model (ALM), Sliding Mesh (SMI) and Multiple Reference Frame (MRF). They found

* Corresponding author
Email: douhaboulla@gmail.com (D. Boulla)

https://doi.org/10.61435/ijred.2025.61437
ISSN: 2252-4940/© 2025.The Author(s). Published by CBIORE

that ALM shows more moderate variation in C_P with TSR and more stable flow, while MRF captures more variation, including stall conditions at TSR = 6 and optimum angle of attack at TSR = 7.5. Meanwhile, (Maronski Ryszard *et al.* 2018) conducted a 2D numerical analysis for unsteady and steady aerodynamic characteristics for the Darrieus turbine composed of two NACA0018 airfoils. The improvement of the actuator cylinder (AC) and double multiple flow tube (DMST) models for a stable and unstable simulation of a vertical-axis aerodynamic rotor with curved deforming blades was carried out by (Kevin R. Moore *et al.* 2020). They concluded that unsteady simulations are 5 to 10 times as rapid, while maintaining accuracy comparable to vortex methods, with speed gains of up to 5000 times. Lositano *et al.* (2019) analyzed the performance of an H-Darrieus rotor equipped with cambered blades and a tubercles leading edge (TLE). CFD simulation results show that TLE reduces lift, increases drag and causes torque inversion, thus degrading wind turbine performance. (Maître *et al.* 2013) presented a 2D RANS CFD numerical model of an H-Darrieus cross flow marine turbine using the ANSYS-Fluent code. (Ying Wang *et al.* 2018) proposed a new geometric design for a Darrieus vertical axis wind turbine with an automatically deformed blade, with the aim of achieving better aerodynamic performance through numerical CFD simulation. Their results show that the low solidity turbine can improve its maximum power coefficient by 14.56%. (Mohammed Shaheen *et al.* 2017) analyzed Darrieus multi-turbine clusters to optimize wind farms. However, a triangular configuration of three turbines improves the power coefficient (C_P) by up to 30% compared with a single turbine. (Zhandos Baizhuma *et al.* 2021) proposed a numerical method for demonstrating the aerodynamic performance of vertical axis wind turbines rotary (VAWTs) under icing conditions by adopting two techniques: MRF, which simulates rotational effects on droplets and ice formation, with ice shapes changing every 36° azimuthal angle, and sliding mesh (SMT), which models the unsteady and rotational effects of the flow field.

A 2D simulation of the aerodynamic performance of an H-Darrieus wind turbine equipped with a rotor designed by the McDonnell Aircraft Company and consisting of three fixed blades, using the URANS method and the SST turbulence model of two independent aerodynamic approaches: the vortex model and the CFD code FLOWER was analyzed by (Krzysztof Rogowski *et al.* 2020). The results show that a maximum power coefficient of 0.5 was obtained for operation with fixed blades. (Mauro *et al.* 2020) proposed a 2D CFD model for an H-Darrieus micro-wind turbine, validated experimentally in a subsonic wind tunnel. However, a hybrid LES/RANS simulation coupled with a transition model proved more accurate than the advanced URANS models. (Chen *et al.* 2024) improved the performance of a vertical-axis H-Darrieus wind turbine (VAWT) with a novel double deflector design. Indeed, their results provided training data to an artificial neural network (ANN) to predict the optimal configuration, showing that the double deflector design improves performance over a bare or single deflector wind turbine. (Boulla *et al.* 2025) studied the aerodynamic performance of an H-Darrieus turbine using 2D CFD simulation, comparing two turbulence models, $k-\varepsilon$ Realizable and $k-\omega$ SST. The results confirm the superiority of the $k-\omega$ SST turbulence model over the $k-\varepsilon$ Realizable model for C_P, with maximum values of 36%, 38% and 35% for velocities of 10, 15 and 20 respectively. (Zhenzhou Zhao *et al.* 2022) explored different strategies for improving the aerodynamic performance of floating VAWTs, focusing on geometric parameter optimization, blade modification, power augmentation devices, hybrid systems and variable pitch control. Qasemi *et al.* (2020) analyzed the power generation performance of a vertical axis, straight bladed wind turbine equipped with a flat plate deflector, using Taguchi's L16 orthogonal lattice-based experimental design method. The results showed that the deflector parameters improved the wind turbine efficiency by 16.42% compared to a model without a deflector.

The energy performance and aerodynamic forces acting on a vertical-axis, straight-bladed Darrieus wind turbine, using CFD and BE-M theory, was evaluated by (Castelli *et al.* 2011). The results show that the instantaneous power coefficient exceeds the Betz limit three times per rotor revolution, compared with the average power coefficient. (Sedaghat *et al.* 2017) formulated the optimum rated wind velocity for continuously operating variable-velocity wind turbines at maximum power coefficient, to maximize annual energy production (AEP). (Wang *et al.* 2012) studied unsteady turbulent flows around an oscillating airfoil inducing dynamic stalls, comparing the URANS approach with the more advanced DES approach. This comparison showed that the DES approach is superior to the URANS approach. (Kanyako *et al.* 2015) investigated the aerodynamic performance of Darrieus small vertical axis wind turbines (VAWTs) for Reynolds numbers between 10^5 and 10^6, comparing two analytical aerodynamic methods: the low-fidelity Double Multiple Streamtube (DMS) method and the mid-fidelity Lifting Line Free Vortex Wake (LLFVW) method. The results show that, as solidity decreases further, the LLFVW method predicts higher values than the DMS method for the entire TSR range. (Bausas *et al.* 2015) studied the performance of a 5 kW VAWT under fluctuating wind conditions using CFD modeling, with symmetrical and cambered blades in 2D. The results show that wind fluctuations have a negative impact on VAWT performance, and a blade with a camber of 1.5% offers the best performance, with an average unstable power coefficient of 0.31, compared with an optimum stable power coefficient of 0.34.

The aim of our study is to improve the aerodynamic performance of the H-Darrieus wind turbine by adding a fairing to our rotor, using CFD simulation with Ansys Fluent software. This approach has not been explored in the aerodynamic literature, which sets it apart from previous studies. In addition, this study focuses on improving the design and performance of components protecting the delicate parts of the H-Darrieus turbine, as well as on optimizing energy efficiency, which is crucial to the competitiveness of renewable energies. Furthermore, after validating our simulation model with that of (Balduzzi *et al.* 2016), a comparison of the two methods Multiple Reference Frame (MRF) and Sliding Mesh (SM) has been carried out concerning the variation of power and moment coefficients as a function of TSR. It can be affirmed that the MRF method provides a higher improvement in the aerodynamic performance of the H-Darrieus rotor, and was applied throughout the rest of the work. Then, a study of lift/drag as a function of angle of rotation and at different chord lengths was adopted to identify the position of the angle that offers the optimum distribution of lift on the blades. To this end, another parametric study was carried out under the addition of a fairing to the H-Darrieus rotor to compare three different fairing geometries at different chord lengths, namely 2.5, 3, 3.5, 4 and 4.5. In addition, velocity, vorticity and pressure contours for the three profiles were presented, taking into account variations and settings of optimal parameters for observing flow and recirculation zones. In addition, the results confirm that the DAE-11 fairing outperforms Eppler 423 and NACA 2412 profiles. Secondly, it improves power and stability, and

minimizes pressure losses caused by vortices around the H-Darrieus rotor, for optimum energy production.

2. Methodology

2.1 VAWT geometric configuration

In this study, the VAWT H-Darrieus geometry was selected based on the configuration proposed by (Balduzzi *et al.* 2016) This configuration, as illustrated in Fig.1, comprises three blades, each designed from a NACA0018 airfoil with a blade chord length of C = 0.246 m, solidity (σ) = 0.44, height (h) = 1 m and diameter (D) = 1.7 m. The blade trailing edge was modified by connecting the upper and lower surfaces of each of the three blades with a 3.80 mm straight line, with the aim of avoiding the generation of mesh elements. The analysis takes into account blade rotation angles θ equal to θ = 45°, θ = 90°, θ = 135°, θ = 180°, θ = 225° and θ = 270°. The rotor is equipped with an external fairing system designed to optimize the performance of H-Darrieus vertical axis aerodynamic turbines. This device, installed around the wind turbine rotor, accelerates airflow, increases stability, covers and protects various turbine components, reducing aerodynamic drag and improving velocity. This manifests itself in better performance, minimizing pressure losses, turbulence and take-offs. In fact, this fairing increases the power coefficient (C_P) and improves the energy performance of the H-Darrieus wind turbine. Different types of airfoils for the H-Darrieus turbine fairing, such as 4-digit NACA, 5-digit NACA, NACA series 6 (Asr *et al.* 2016), Wortmann, ONERA and DU, are used to optimize turbine aerodynamics, maximizing lift and minimizing drag. This retains the idea of adopting NACA 2412, Eppler 423 and DAE-11 airfoils for their specific advantages on H-Darrieus turbines enveloped by a fairing system. The NACA 2412 profile is simple and reduces drag at high Reynolds numbers (Re) (Chunyan *et al.* 2023). Then the Eppler 423 profile offers adequate advantages due to its low thickness. It is also optimized for a low angle of attack, which contributes to reducing performance losses due to variations in blade orientation relative to the air (Chandra *et al.* 2020). It is particularly useful in conditions where it is essential to reduce turbulence and improve efficiency at various velocities. For the DAE-11 profile, especially used in complex flow situations and at low velocities, its main objective is to reduce drag while maintaining a high lift coefficient. However, its camber improves the turbine performance at low angles of attack (α°) and enhances its stability in configurations where turbulence must be reduced. A comparison between these three profiles NACA2412, Eppler 423 and DAE-11 was carried out in order to identify the one that generates the most relevant and best-adapted efficiency for the H-Darrieus turbine, by varying many parameters. On the other hand, profile DAE-11 offers better performance on all parameters.

2.2 Calculation domain and boundary conditions

The 2D computational domain for simulating the aerodynamic performance of the H-Darrieus rotor, with and without fairing, is shown in Fig. 1. At the inlet, the length is placed at 40D from the center of the turbine, for the outlet, it is placed at 40D and the width of the domain has been set at 60D. The boundary conditions were defined using uniform free stream velocity and pressure, they are characterized as follows: an initial free stream velocity U_∞ = 8 m/s at the inlet, and none atmospheric pressure at the outlet. The fluid used in this study is air with a density (ρ) of 1.225 kg/m^3, at a temperature of 300 K, and a dynamic

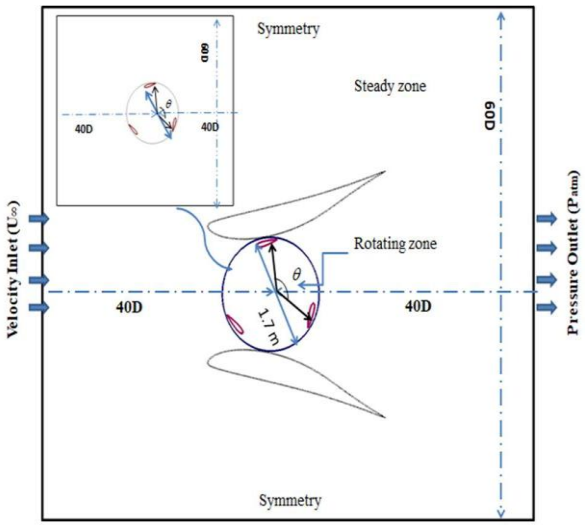

Fig. 1 Geometric configuration of the calculation zone.

viscosity (μ) of 1.7894 × 10^{-5} kg/m.s, a turbulence intensity of 3%. These values are used to validate our model (Balduzzi *et al.* 2016). No slip wall interaction conditions were applied at the interfaces to the blade surface and fairing (Mahdi *et al.* 2016) The multiple reference frames (MRF) mesh technique was applied to simulate the rotational motion of the H-Darrieus turbine rotor in steady state (Peter *et al.* 2011). On the other hand, the computational domain is separated into two regions, a rotating one in the form of a cylinder including the three turbine blades, and a stationary one in the form of a rectangle including the three types of fairing delimited by interfaces and created by the ANSYS 2022 R1 software (Inc, A. 2020; Fluent, A. 2020). Symmetry boundary conditions are applied to the upper and lower sides of the domain. Furthermore, the blades are modeled as a rotating domain due to their motion in relation to the rotor. It is important to note that these boundary conditions have facilitated the simulation of appropriate flow conditions, favoring the progression of the flow and the convergence of the solution towards a realistic model.

2.3 Performance indicators

The simulation is carried out for tip speed ratios (TSR) between 1.1 and 3.3. This is achieved by fixing the incoming free velocity flow at (10 m/s) while varying the position angle rotor (θ°) and angle of attack (α°) for the fairing section, as shown in equation (1) (Willmott *et al.* 1985).

The tip speed ratio (TSR) as a key parameter in turbine aerodynamic and is a parameter describing the motion of the rotor in H-Darrieus. It is represented by the following equation (1):

$$TSR = \frac{\omega R}{U_\infty} \quad (1)$$

Where ω is the angular velocity, R is the radius of the turbine and U_∞ is the free stream velocity wind.

Most researchers focus on numerical and experimental studies to optimize the power coefficient (C_P) of the H-Darrieus turbine and approaching their performance at the Betz limit of 60%. In addition, the torque coefficient (C_m) is a performance indicator, measuring the rotor's capacity to transform incoming wind energy into mechanical torque (Ahmed *et al.* 2022).

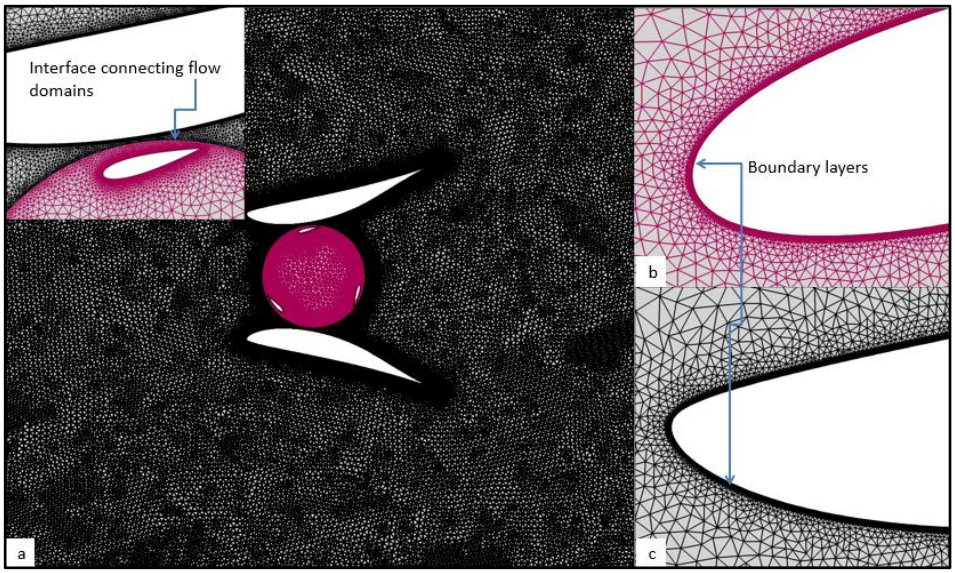

Fig. 2 (a) Hybrid mesh of the rotor domain. (b) Boundary layer size applied to the fairing walls. (c) Boundary layer size applied to the walls of the NACA0018 airfoil.

The performance coefficients can be expressed using equations (2, 3) (Paulo *et al*. 2021).

$$C_m = \frac{M_t}{0{,}5\rho U_\infty^2 AR} \tag{2}$$

$$C_P = \frac{P_t}{0{,}5\rho U_\infty^3 A} = TSR \times C_m \tag{3}$$

With A is the section covered by the wind, M_t is rotor torque indicator and P_t is power.

2.4 Mesh independence analysis

The meshing of all the surface of the H-Darrieus turbine, including the leading and trailing edges is produced using ANSYS Workbench software. A hybrid mesh (quadrilateral and triangular) was selected in this study because of its flexibility and ability to reduce the number of mesh elements, with applied refinement in the computational domain, as shown in Fig. 2, to ensure high mesh quality near the walls and to optimize accuracy. This approach makes it possible to create highly accurate meshes, which are essential for detailed aerodynamic analysis of Darrieus wind turbines using CFD software. The impact of mesh quality on the precision and reliability of performance coefficient results remains to be thoroughly investigated in order to ensure reliable solutions.

The $k-\omega$ SST turbulence model requires that y+ be between 1 and 5. In our case, we set y+ to 1 to estimate the first adjacent layer to the wall. On the other hand, the growth rate mesh size around the aerodynamic profiles and the fairing was set between 1 and 1.2. The mesh is particularly fine near the walls, as Fig. 2 clearly shows. In order to optimize Computational Fluid Dynamics (CFD) computational costs while guaranteeing a good representation of flow phenomena, it was necessary to modify the mesh size. The main difference between the different mesh types lies in the grid size around the blade and fairing. The minimum grid sizes taken into account around the blade are 2.9×10^{-5} m, 1.2×10^{-5} m and 3.5×10^{-6} m respectively, thus corresponding to the so-called coarse, medium and fine meshes. In addition, the boundary layer associated with the mesh was generated with 25 cell layers and a cell growth ratio of 1.2. The Reynolds number calculated for this study, based on the diameter of the H-Darrieus rotor, is approximately $Re = 1.2 \times 10^6$.

Furthermore, the independent grid was determined as a function of the power coefficient (C_P) for the 2D turbine, as shown in Fig. 3. This analysis examines the variation of the power coefficient (C_P) as a function of the number of elements for a tip-speed ratio TSR = 2.5. However, when evaluating the variations in C_P, a difference was observed between a medium mesh and a fine mesh, with a maximum variation of 0.78%. A sensitivity study was carried out using the following four meshes 100000, 152000, 175000, and 230000 elements. It can be observed that the power coefficient increases as the number of mesh elements increases from 100000 to 175000 elements, becoming almost constant from 175000 elements. It can therefore be concluded that the coefficient becomes stable from the value of 175000 elements, and the solution becomes independent of the grid from this value.

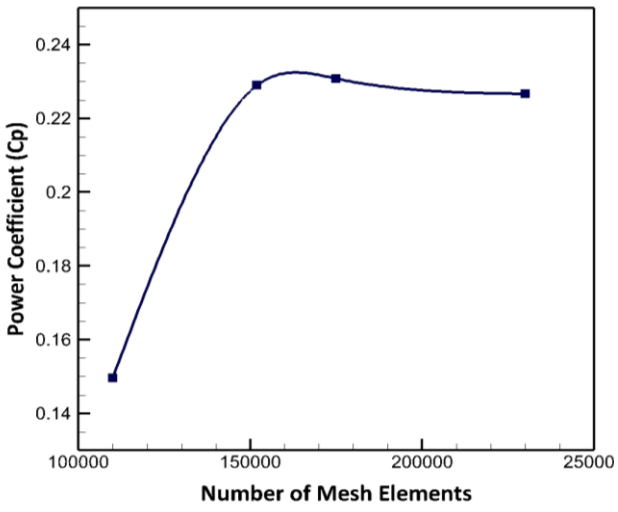

Fig. 3 Variation of C_P with number of mesh elements.

2.5 Solver settings

The numerical modeling parameters used to study the flow around the turbine, including the RANS approach for incompressible 2D flow with Fluent CFD software, are detailed in this section. This approach, which is commonly used on an industrial scale, offers greater efficiency and lower computing costs than other models such as LES, DNS and many others. The coupled algorithm is applied to solve the pressure-velocity coupling and accelerate CFD model convergence. The second-order upwind scheme was adopted for the spatial discretization of the RANS equations, and the second-order scheme for the temporal discretization, in order to achieve more accurate and reliable prediction of CFD numerical simulations (Saïf ed-Dîn *et al*. 2023). A high number of inner-iterations (1000 iterations) were used to ensure convergence of the solution. In addition, the $k-\omega$ SST turbulence model is used to solve the Navier-Stokes equations, a model particularly adapted to the analysis of flow around H-Darrieus rotors due to its optimization in treatment complex boundary layer problems. The rotation domain of the H-Darrieus turbine was simulated using the multiple reference frame (MRF) technique (ANSYS Inc 2014; Celik *et al*. 2020). The aim is to ensure optimum resolution of the dynamics and reduce computing time, while providing a sufficiently reliable solution. The elementary degree of rotation was fixed at 1°, a value selected on the basis of simulations carried out (Fluent 2011). In addition, a y+ value of 1 was selected to guarantee optimum resolution of the viscous sublayer near the wall.

2.6 Sliding Mesh and MRF Methods

The sliding mesh technique was employed to simulate the interaction between the fixed and rotating fluid zones of the H-Darrieus rotor. This approach necessitates an unstable calculation and generates time-varying results instead of time-averaged ones. This method is used to compare it with the MRF method. The integral form of the equation can be expressed as follows (Fluent 2011).

$$\frac{d}{dt}\left(\int_V \rho\phi dV\right) + \int_{\partial V} \rho\Phi\left(\vec{u}-\vec{u}_g\right)d\vec{A} = \int_{\partial V} \Gamma\nabla\Phi d\vec{A} + \int_V S_\phi dV \quad (4)$$

Where, ρ is the air density, $u$is the flow velocity, u_g is the mesh moving velocity, Γ is the diffusion coefficient and S_ϕ is the source term of Φ.
The time derivative term in Eq. (4) is written as presented in Eq. (5)

$$\frac{d}{dt}\left(\int_V \rho\phi dV\right) = \frac{[(\rho\Phi V)^{n+1}-(\rho\Phi V)^n]}{\Delta t} \quad (5)$$

Where n and (n + 1) respectively denote the quantity at the current time level tn and the next time at tn+1. The volume of the temporal level (n + 1), V^{n+1} is calculated from Eq. (6) (Versteeg 2017).

$$V^{n+1} = V^n + \frac{dV}{dt}\Delta t \quad (6)$$

Where $\frac{dV}{dT}$ is the volume time derivative.
The temporal rate of change of cell volume is zero and Eq. (6) can be simplified to Eq. (7) (Versteeg 2017).

$$V^{n+1} = V^n \quad (7)$$

Indeed, Eq. (5) becomes Eq. (8) (Versteeg 2017).

$$\frac{d}{dt}\left(\int_V \rho\phi dV\right) = \frac{[(\rho\Phi)^{n+1}-(\rho\Phi)^n]V^n}{\Delta t} \quad (8)$$

The Multiple Reference Frame (MRF) approach is a stationary method used in Computational Fluid Dynamics (CFD) to model systems with rotating configurations. This technique considerably reduces computation time while efficiently providing a sufficiently accurate solution. It is thus characterized by its low computational cost, while offering a satisfactory solution for the majority of industrial applications. The method assumes that fluid flow in each reference frame follows the Navier-Stokes equations with Coriolis and centrifugal forces. The grid is maintained fixed during the calculation. This is equivalent to freezing the motion of the moving part at a given position and analyzing the instantaneous flow field with the rotor (Menter 1994).

2.7 Mass and momentum equations

The fluid around the blades is considered incompressible and is described by the conservation equations of mass and momentum in steady state, using the MRF method. These equations can be written in vector notation as follows (Menter 1994; Marini *el al*. 1992):

The mass conservation equation:

$$\nabla.(\rho\vec{u}) = 0 \quad (9)$$

The momentum conservation equation:

$$\nabla.(\rho\vec{u}\vec{u}) = -\nabla P + \nabla.\tau + \rho\vec{g} \quad (10)$$

Where P is the static pressure, is τ the stress tensor,
The stress tensor τ is described by:

$$\tau = \mu\left((\nabla\vec{u} + \nabla\vec{u}^T) - \frac{2}{3}\nabla.\vec{u}I\right) \quad (11)$$

Where, μ is the molecular viscosity and I is the unit tensor.

2.8 SST k-omega turbulence model

The $k-\omega$ shear stress transport (SST) turbulence model is a type of hybrid model, combining two models to calculate the flow in the near-wall region. The turbulent kinetic energy k and the specific dissipation rate ω are obtained from the following transport equations (12) and (13), according to the proposals of (Hoseinzadeh *et al*. 2020; Vennell *et al*. 2013):

$$\frac{\partial}{\partial x_i}(\rho k u_i) = \frac{\partial}{\partial x_j}\left(\Gamma_k\frac{\partial k}{\partial x_j}\right) + G_k - Y_K + S_K + G_b \quad (12)$$

$$\frac{\partial}{\partial x_i}(\rho\omega u_i) = \frac{\partial}{\partial x_j}\left(\Gamma_\omega\frac{\partial \omega}{\partial x_j}\right) + G_\omega - Y_\omega + S_\omega + G_{\omega b} \quad (13)$$

G_k is the generation kinetic energy production of turbulence due to mean velocity gradients, G_ω is the generation of ω, Γ_k and Γ_ω represent the effective diffusivity of and ω respectively, S_k and S_ω are user-defined source terms, G_k and $G_{\omega b}$ represent the buoyancy terms.

The turbulent viscosity is defined using Eq. (14).

$$\mu_t = \frac{\rho k}{\omega} \frac{1}{max[1/\alpha^*, SF_2/a_1\omega]} \quad (14)$$

With:
S is the magnitude of the strain rate

α^* is defined in eq. (15).

$$\alpha^* = \alpha^*_\infty \left(\frac{\alpha^*_0 + Re_t/R_k}{1 + Re_t/R_k}\right) \quad (15)$$

$$Re_t = \frac{\rho k}{\mu\omega}, R_k = 6, \alpha^*_0 = \frac{\beta_i}{3}, \beta_i = 0.072$$

When the Reynolds number of the $k-\omega$ model is high $\alpha^* = \alpha^*_\infty = 1$

$$F = tanh(\emptyset_2^2) \quad (16)$$

And,

$$\phi_2 = max\left(2\frac{\sqrt{k}}{0.09\omega k}, \frac{500\mu}{\rho y^2 \omega}\right) \quad (17)$$

Where y is the distance to the next surface.

3. Validation

In order to assess the reliability of the results obtained from the CFD simulation, experimental measurements carried out by (Balduzzi *et al.* 2016) were used to verify the conformity of the model presented. The geometric model proposed by (Balduzzi *et al.* 2016) consists of an H-Darrieus rotor, where each blade is equipped with a NACA0018 profile. This model has several specific characteristics namely a diameter of D = 1.7 m, a strength of σ = 0.44 and a chord length of C = 0.246 mm. This wind turbine operates at different tip speed ratios (TSR) with a free velocity flow of U_∞ = 8 m/s and a turbulence intensity of 3%. The boundary conditions of the domain were defined so as to reproduce the experimental conditions. The power coefficient C_P was selected as the optimization function with respect for the following tip speed ratios: TSR = 1.1, TSR = 1.7, TSR = 2, TSR = 2.2, TSR = 2.5, TSR = 2.8 and TSR = 3.3 for the evaluation of the results.

Figure 4 shows a validation study of the model in comparison with the experimental study and CFD simulation performed by (Balduzzi *et al.* 2016), as well as with the CFD simulation results of the previous work by (Boulla *et al.* 2025) and the present one. The main objective of this study is to compare the MRF method adopted in the present work with the Sliding Mesh method used by (Balduzzi *et al.* 2016) and (Boulla *et al.* 2025), by analyzing the variation of C_P as a function of TSR. To facilitate understanding of the comparison between the present results and the previous results from (Boulla *et al.* 2025) and (Balduzzi et al. 2016), the obtained results are validated using the relative error (RE) method expressed by the equation below (18) (Qasemi *el al.* 2020). This method combines the power coefficient ($C_{P_{exp,i}}$) obtained experimentally by (Balduzzi *et al.* 2016) and the power coefficient ($C_{P_{sim,i}}$) referring to numerical simulations. This method is used to calculate the difference between simulation results and experimental data. However, the results show that (Balduzzi *et al.* 2016) obtained a relative error for the CFD simulation of 13%, (Boulla *et al.* 2025) a relative error of 11% for the Sliding Mesh method, while our CFD study which imposes on the MRF method presents a relative error of 5%. We can conclude that the C_P values we obtained through the use of the MRF method are close to those

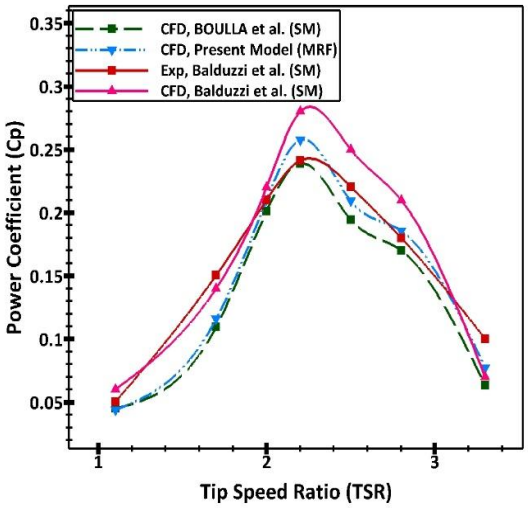

Fig.4 Validation of the MRF and Sliding Mesh methods.

obtained by (Balduzzi *et al.* 2016) compared to the use of the Sliding Mesh method, indicating a good correlation with the experimental results.

$$ER = \frac{1}{n}\sum_{i=1}^{n} \frac{\left|C_{P_{exp,i}} - C_{P_{sim,i}}\right|}{C_{P_{exp,i}}} \times 100 \quad (18)$$

The results also show that an error of 22% was recorded in the CFD study using the MRF method at a low TSR value of 1.7, compared with other studies where the Sliding Mesh method was used. It is shown that better performance is offered by the MRF method when used at high TSR values (Maalouly *et al.* 2022; Gemayel *et al.* 2023). On the other hand, it is observed that the increase in TSR, particularly at higher steady-state speeds, leads to more stable and predictable effects, which explains the reduction in errors observed at higher TSR values. MRF simulations are distinguished by their ability to deliver faster and more reliable results, while reducing calculation time and maintaining sufficient accuracy. At significant TSR values, the blade rotation velocity becomes much greater than the free stream velocity, allowing the blades to operate in a range where more effective lift is generated. This enhances the aerodynamic profile and optimizes energy performances.

That the MRF method obtained is sufficient to study the aerodynamic performance of H-Darrieus vertical axis wind turbines (VAWT). It is also better than the sliding mesh method, and will therefore be adopted in the rest of our work to optimize energy efficiency.

4. Results and discussion

4.1 Influence of chord length and azimuth angle position on C_D and C_L

This study focuses on optimizing the aerodynamic performance of the fairingless H-Darrieus rotor, using CFD modeling and the MRF numerical method. This method enables us to model dynamic fields, in particular velocity and pressure, and converge on a stable, accurate solution.

The variation of drag coefficient (C_D) with position angle θ, for different values of blade chord length of type NACA0018 namely 0.246 m, 0.375 m and 0.850 m are shown in fig. 5 (a).

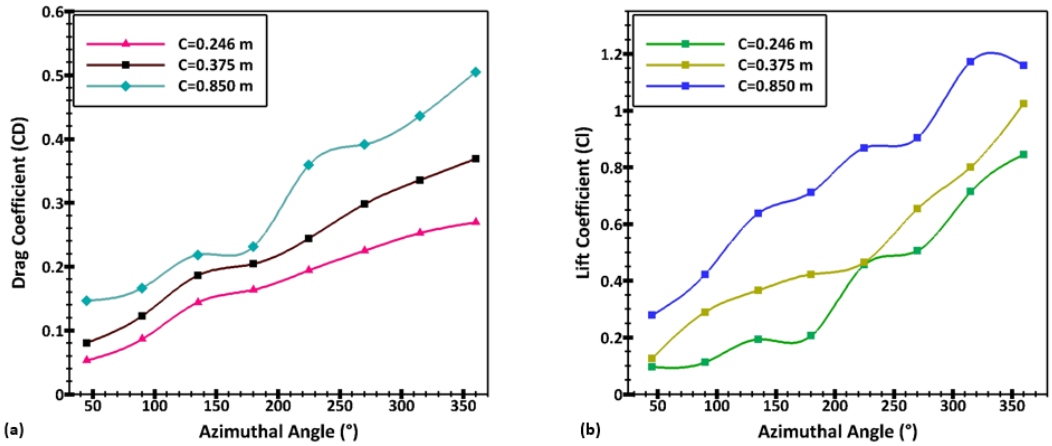

Fig.5 Variation of instantaneous drag and lift coefficients: (a) (C_D) as a function of the azimuth angle, (b) (C_L) as a function of the azimuth angle for different chord lengths.

This analysis was carried out to investigate the aerodynamic effects between different blade chord lengths and airflow, using CFD (Computational Fluid Dynamics) simulation and the MRF method. This figure shows that C_D increases with increasing position angle, regardless of chord length. It also shows that this drags coefficient increases with increasing chord length, reaching values of 50%, 37% and 27% for chord lengths of 0.850, 0.375 and 0.246 respectively, at θ = 360°. We also observe that the influence of chord length is greater for larger values of θ. This is due to aerodynamic disturbances in the form of vortices and turbulence formed behind the blades. Moreover, higher drag indicates increased energy loss.

Flow detachment is caused when air flowing around the H-Darrieus rotor becomes detached from the surface of the NACA0018 blade, particularly as position angles and chord lengths are increased. Turbulence, energy loss, and increased drag can be caused as a result. On the other hand, when the position angle and chord length are optimized, the air remains stuck to the surface of the blade, and a stable tangential velocity is maintained. This ensures that the turbine is reliably and efficiently turned by the blade, while drag is reduced.

The evolution of lift (C_L) is shown in fig. 5 (b) as a function of azimuth angle positions for different chord lengths. From this figure, we can see that the lift coefficient (C_L) increases approximately by 85% with a chord length of 0.246 and by 102% with a chord length of 0.375. It also increases with the angle of rotation, reaching a maximum value at θ = 360°. Furthermore, for a chord length of C = 0.850, the lift coefficient is increased up to 117% at θ = 315°, then decreases for θ between 315° and 360°. It can be deduced from this that the lift coefficient is increased with position angle and chord length, although for larger position angles, a decrease tends to occur. This is caused by aerodynamic stall, which can make the blades less efficient and the turbine energy performance reduced. On the other hand, more lift can be generated by a turbine equipped with long-chord blades, thus improving blade efficiency and reducing the risk of dynamic stall. However, an increase in drag can also be caused if aerodynamic factors are not properly

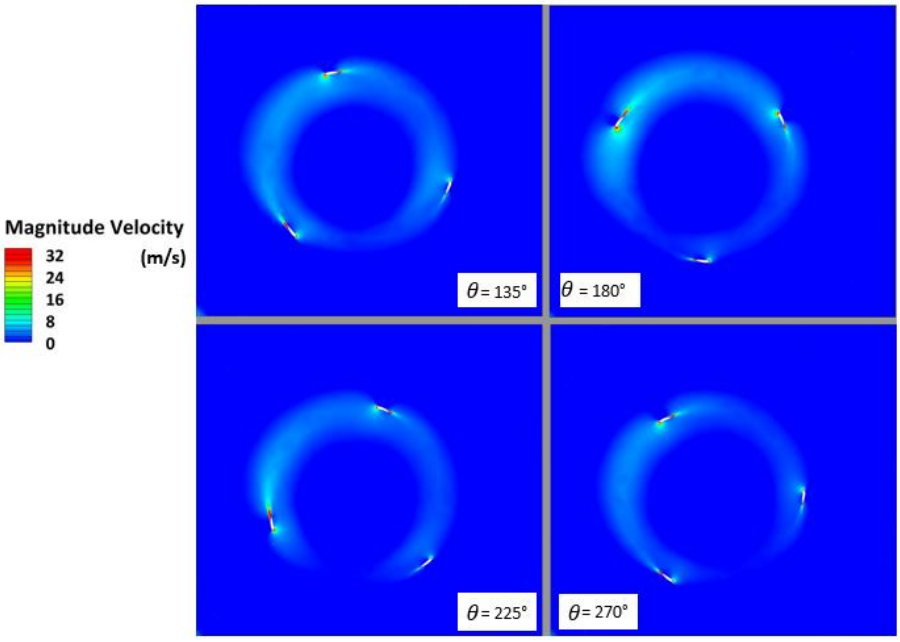

Fig.6 Magnitude velocity contours at different azimuth angles for C = 0.246, TSR = 3.3.

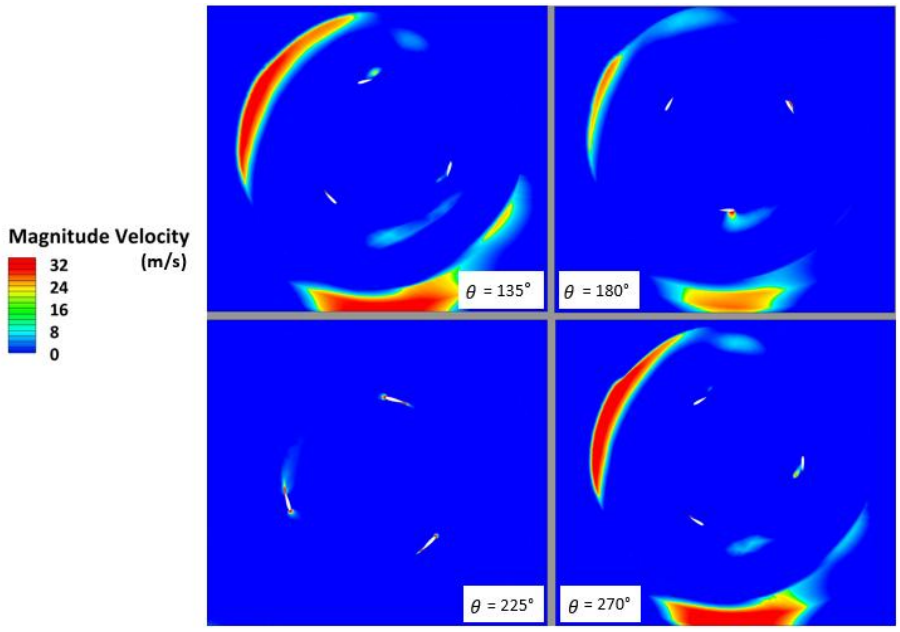

Fig.7 Magnitude velocity contours at different azimuth angles for C = 0.375, TSR = 3.3.

optimized, and excessively high drag can become a limiting factor in turbine energy efficiency. This result was also found by (Qamar *et al*. 2023), who showed that cambered blade designs with long chord lengths maximize performance and reduce the negative effects of turbulence.

Figures 6, 7 and 8 show a detailed analysis of velocity field distributions around the fairingless H-Darrieus wind turbine, for different chord lengths and at four rotation angle positions equal to 135°, 180°, 225° and 270°, at TSR = 3.3 and for U_{∞} = 10 m/s. This study aims to assess the impact of blade azimuth angle and chord length on interactions, in terms of aerodynamic forces and dynamic behavior under the influence of wind.

Figure 6 illustrates the displacement of air along the edges of the H-Darrieus rotor blades, whose chord length is equal to 0.246. In addition, we observe the formation of circular vortices around the rotor, at all the position of the angle of rotation. These vortices move along the length of the blades, generating high-velocity zones near the leading edge. This contributes significantly to lift. As a result, a significant proportion of the wind is redirected towards the lower surface of the blades, leading to the formation of pressure zones higher than those on the upper surface, as a result of the increased pressure in this zone. This redistribution of pressure reduces lift and increases drag, upsetting the airflow balance around the blades (Fig. 5). This disruption has the effect of altering the global aerodynamic flow efficiency of the H-Darrieus rotor. In addition, between 225° and 270°, there is a decrease in pressure between the lower and upper surface of the blade. This pressure difference,

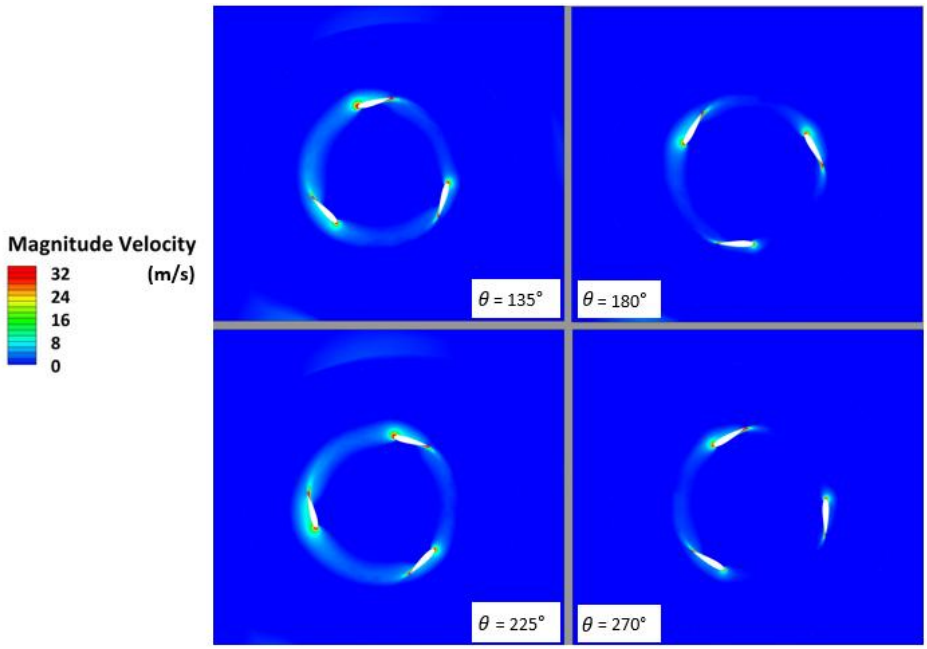

Fig.8 Magnitude velocity contours at different azimuth angles for C = 0.850, TSR = 3.3.

induced by the higher air velocity on the upper surface, generates a lift force, as explained by (Milad Yousefi Roshan *et al.* 2021).

In contrast, the velocity contour shown in Fig. 7 reveals the flow from aerodynamic profiles with chord lengths equal to 0.375. At $\theta = 135°$, a vortex is begun to form at the back of the blade, but most of the flow remains attached to the surface. At $\theta = 180°$, vortex separation is observed at the trailing edge of the blade as it is rotated at high speed. This is caused when the boundary layer is detached from the blade surface, resulting in the airflow flowing non-uniformly. The air then moves in the form of vortices, which can lead to a loss of rotor performance. At $\theta = 225°$, the flow remains predominantly attached, with a lower number of vortices observed and relatively stable flow dynamics, which is favourable to lift. At $\theta = 270°$, although some areas of slightly higher pressure may appear, performance is begun to be generated by the blade for the next rotation to an optimal TSR equal to 3.3, thus promoting rotor efficiency (Fig. 5).

A convergence of the velocity contour associated with the reorganization of the fluid flow accelerated by the blades is illustrated in Fig. 7. However, the stabilization around the blades and the accuracy of the simulations, as well as their ability to capture complex phenomena such as flow acceleration on the upper surface and flow separation, are observed by visual examination of the velocity contours. This is because, as the rotor rotates, the air pressures decrease at the surface of the blades and the air moves at a higher velocity around them, causing acceleration and a decrease in pressure, which means that the fluid accelerates in this region and the velocity increases. On the other hand, the physical behavior of the H-Darrieus turbine studied is accurately reflected by the results obtained. In Fig. 8, the blade chord is 0.850. However, the flow remains attached and stable to the blade surface in all rotational positions, generating a dense vortex around the rotor. It is suggested that the turbine undergoes less mechanical stress, allowing more energy to be generated for a TSR equal to 3.3. In short, long chord blades are more efficient than medium chord blades at traversing vortices.

The velocity contours reveal the flow distribution and vortex structures around the rotor, particularly at the leading and trailing edges of the blades. At a chord of 0.246, much of the wind is redirected towards the lower surface of the blades, resulting in an increase in pressure relative to the upper surface. This redistribution of pressure reduces lift while increasing drag, thus perturbing the balance of airflow around the rotor. On the other hand, for a chord of 0.375, a convergence of velocity curves was observed during rotor rotation. Air pressure decreases at the surface of the blades and the air accelerates around them, leading to a decrease in pressure, an increase in lift and an improvement in the wind turbine's aerodynamic performance. The flow remains attached and stable at the blade surface. In conclusion, the velocity curves show that the rotor rotates without major interruption, indicating that the H-Darrieus wind turbine operates efficiently and achieves a high-power coefficient.

This highlights the importance of choosing an optimum blade chord length to improve turbine efficiency, as confirmed by the results obtained by (Maalouly *et al.* 2022). These results reveal that the parameters of the fairing's geometric configuration, in particular opening angle α and chord length, influence the aerodynamic performance of the H-Darrieus turbine.

4.2 Influence of the fairing on the H-Darrieus rotor aerodynamic performance

The study focuses on improving the aerodynamic performance of the H-Darrieus rotor, by highlighting the effect of the fairing at different chord lengths C on the power coefficient, according to an angle of attack ($\alpha°$) equal to 0°, a free flow velocity U_∞ = 10 m/s and using the MRF method. In contrast, Fig. 9 (a) shows the variation of the power coefficient (C_P) as a function of TSR, for five distinct values of chord length and in the case of a NACA2412-type fairing.

The results show that maximum C_P values are observed at TSRs of 2.2 and 2.5 for all chord lengths. Subsequently, a decrease in C_P is observed for TSR values between 2.8 and 3.3. More precisely, the power coefficient reaches a higher maximum value of 0.561 for C = 3, at TSR = 2.5. Fig. 9 (b) compares the performance of the H-Darrieus rotor at different chord lengths of the fairing, which is of the Eppler 423 type. However, it can be seen that the power coefficient reaches the maximum value of 0.580 for a chord length of 3 and TSR = 2.5. On the other hand, for TSR equal to 1.1 and 3.3, the power coefficient (C_P) leads to minimum values, regardless of the length considered.

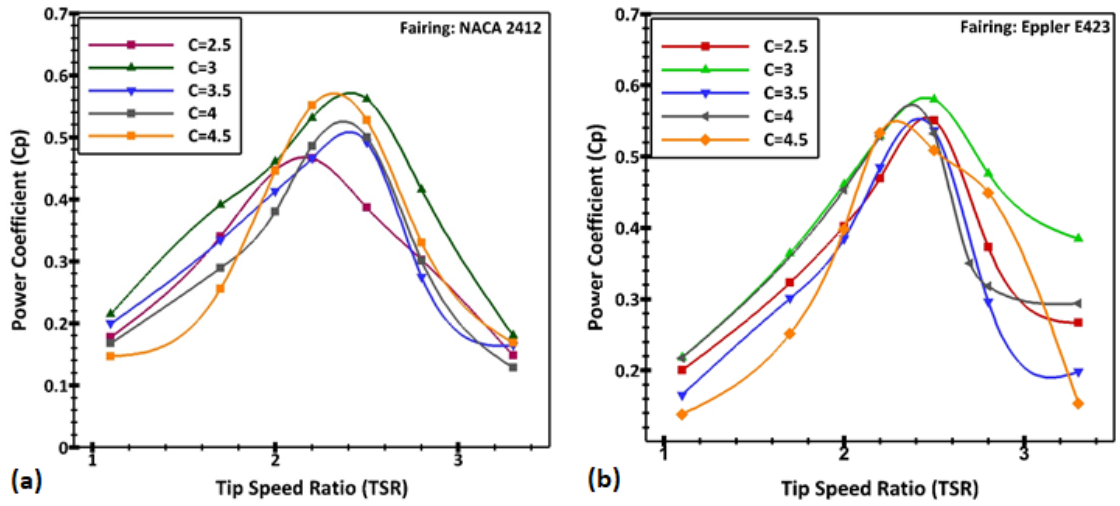

Fig.9 Variation of C_P as a function of TSR for two types of fairings. (a) - NACA2412, (b) Eppler 423, at different chord lengths (C).

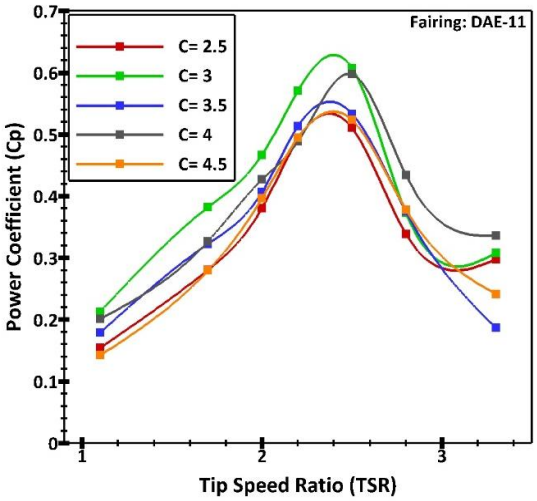

Fig.10 Variation of C_P as a function of TSR for a DAE-11 fairing at different chord lengths (C).

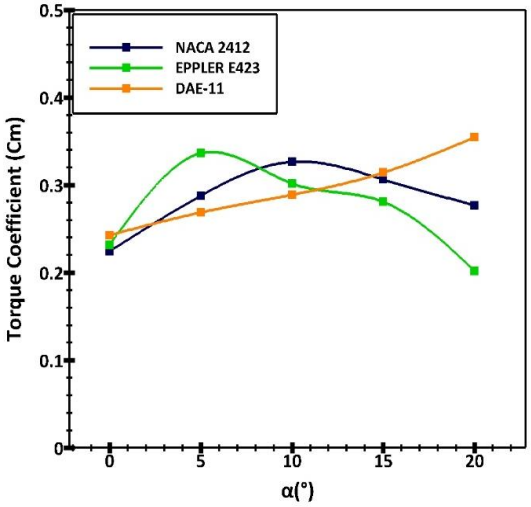

Fig.11 Variation of C_m as a function of angle of attack (α°) for the three fairing types at C = 3 and TSR = 2.5.

Figure 10 performs a similar analysis at different chord lengths of the DAE-11 type fairing. The analysis shows that the maximum peaks of the power coefficient (C_P) are observed with values of 0.607, 0.597, 0.533, 0.523 and 0.510 for a chord length of 3, 4, 3.5, 4.5 and 2.5 respectively at TSR = 2.5. These values then decrease progressively as TSR equals 2.8, 3.3. A comparison of the three maximums power coefficient values of the three fairing profiles at C = 3 and a TSR of 2.5 shows that the DAE-11 type offers better performance. This means that optimizing turbine performance depends on the choice of fairing type and its dimensions during the turbine conception phase. An appropriate fairing configuration enables more efficient use of the flow around the H-Darrieus rotor, which improves energy efficiency.

Based on this detailed analysis of the power coefficient (C_P) as a function of TSR, several conclusions can be drawn regarding the interaction between the H-Darrieus turbine and the NACA2412, Eppler 423, and DAE-11 fairings, as well as their efficiency and aerodynamic behavior. It is generally indicated by the results that turbines equipped with fairings of varying chord lengths have a significant impact on the C_P. However, a higher C_P is shown by turbines with an optimal fairing length of 3 at low and medium TSR for all three types. The conclusion is that this type of fairing improves efficiency and maximizes the wind turbine aerodynamic performance. On the other hand, fairings with a shorter chord length can create an imbalance in relation to the rotor diameter, which can generate rotor instability and perturb turbine flow (Fig. 9,10). This analysis emphasizes the importance of ensuring a balance between the fairing size and rotor characteristics to maintain aerodynamic optimization and prevent negative consequences on H-Darrieus turbine performance, while avoiding excessive drag and energy losses.

In comparison with the results of (Fertahi *et al.* 2023), it appears that the Eppler 420 profile offers better overall performance in terms of power coefficient C_P, particularly at the optimum chord length of C = 4.0R. Whereas the lowest performance is noted for C = 2.5R. In fact, the Eppler 420 profile stands out for its ability to maintain a good lift/drag ratio as well as optimal pressure, which promote better hydrodynamic efficiency. In addition, our study shows that the Eppler 423 airfoil offers significant flow control advantages, minimizing flow separation and reducing vortex-related loss of efficiency, but the DAE-11 airfoil remains the best performing airfoil for this fairing turbine application, particularly in terms of stability and optimization of power output for chord lengths equal to 3.

Figure 11 illustrates the comparison between the three fairings NACA2412, Eppler 423 and DAE-11 regarding the performance of the moment coefficient (C_m) as a function of five angles of attack α = 0◦, α = 5°, α = 10°, α = 15° and α = 20° for the optimum value of the chord C equal to 3 and for TSR= 2.5. However, the NACA2412 profile shows a maximum moment coefficient of C_m = 0.326 at α = 10°, while the minimum value of C_m = 0.224 appears at α = 0°. In addition, the values of C_m initially increase with the angle of attack until α = 10° and then gradually decrease until reaching a value α of 20°. However, for the Eppler 423 profile, the maximum moment coefficient of C_m = 0.336 is reached at α = 5°, while the minimum value of C_m = 0.202, is found at α = 20°. We conclude that C_m values increase until reaching a maximum at α = 5°, then they decrease at the point of α = 20°. In contrast, for profile DAE-11 the moment coefficient (C_m) attains its highest value of C_m = 0.354 at α = 20°. In this context, C_m values increase progressively with increasing angle of attack α. On the other hand, the NACA2412 fairing achieves its optimum efficiency at an angle of attack of α = 10°, while the Eppler 423 fairing at α = 5°, moreover the DAE-11 fairing obtains its best efficiency at α = 20°. This comparison shows that the DAE-11 fairing outperforms the Eppler 423 and NACA2412 profiles, particularly at higher angles of attack. This demonstrates the importance of fairing type selection in maximizing the aerodynamic performance of the vertical-axis H-Darrieus rotor.

The angle of attack allows the fairing to generate a tangent force that propels it forward, improving efficiency and maximizing turbine productivity and durability. However, an optimum angle of attack must be precisely chosen to avoid a sudden drop in lift, while reducing drag and maximizing the moment coefficient (Fig. 11). However, the long-term reliability of the H-Darrieus turbine is ensured by careful management of the angle of attack. The vorticity contours magnitude, as determined by 2D CFD modeling, is shown in Fig. 12 for three fairing chord lengths. Notably, $C_{Fairing}$ = 2.5 (low), $C_{Fairing}$ = 3 (high) and $C_{Fairing}$ = 4 (medium) are integrated into the H-Darrieus rotor, which is comprised of three NACA0018 profiles, each having a low chord length of C = 0.246. This value was utilized to optimize rotor performance through the use of a fairing. However, for the NACA2412 profile of the two $C_{Fairing}$ chord lengths equal to 2.5 and 3, the recirculation zones are on

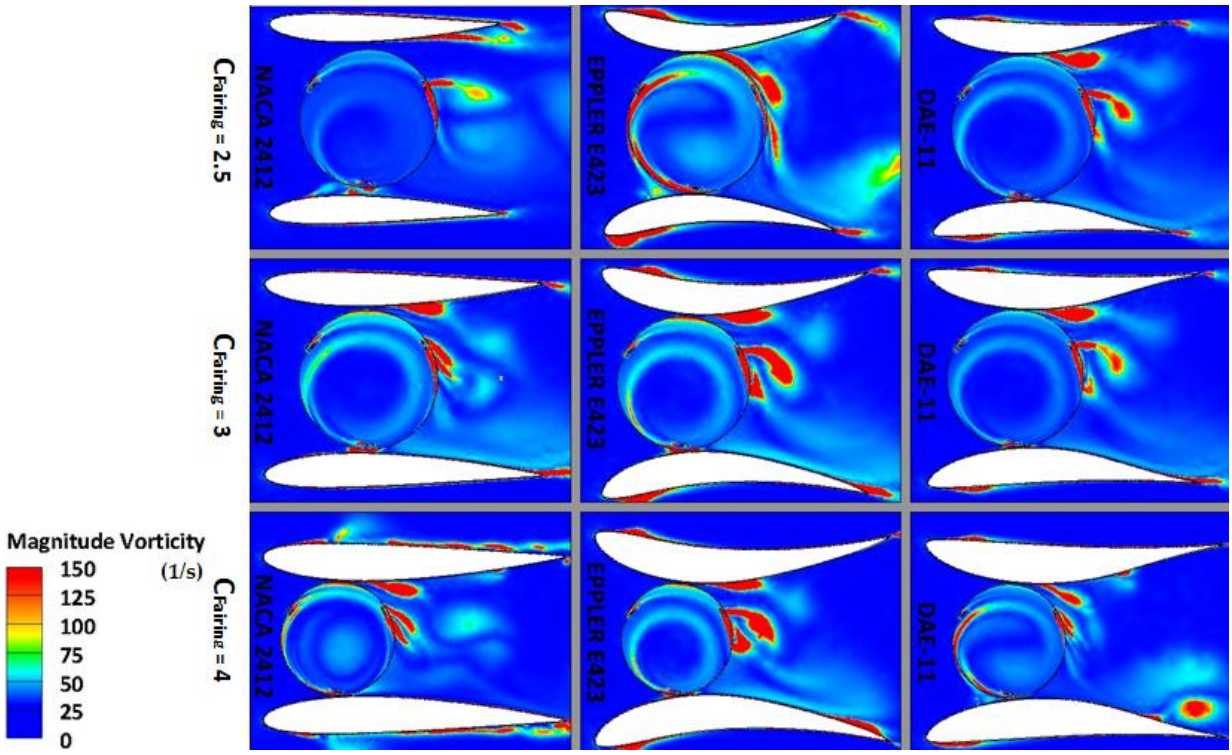

Fig.12 Vorticity contours around the careened H-Darrieus for different values of $C_{Fairing}$ chord length, at θ = 180°, α = 0° and for TSR = 2.5.

the external side of the rotor, indicating that the flow around the turbine is stable, which means that the turbine blades can generate maximum lift due to VAWT efficiency optimization. The recirculation zones expand and move towards the trailing edge of the profile, forming vortices that suggest more complex dynamics with the aerodynamic profile of the turbine. However, for the Eppler 423 profile at $C_{Fairing}$ = 3 and $C_{Fairing}$ = 4, the flow outside the turbine is stable. On the other hand, at $C_{Fairing}$ = 2.5 the recirculation zones progressively enlarge and approach the trailing edge, which can result in efficiency losses and a drop in lift. In the context of the DAE-11 profile, at $C_{Fairing}$ = 2.5 and $C_{Fairing}$ = 3, the recirculation zones do not fluctuate outside the rotor, and this does not perturb the flow of air entering the turbine NACA0018 profile blades. However, at $C_{Fairing}$ = 4 the recirculation zones approach the fairing trailing edge, creating vortices that serve to reduce rotor performance. On the other hand, as the fairing chord length increases, the complexity of the flow increases, this can contribute to a loss of efficiency.

The introduction of different chord lengths (short at low value, medium at high value and long at medium value) into the H-Darrieus rotor design is considered crucial to understand the impact of these variations on aerodynamic performance (Fig. 12). It is suggested that a short chord length fairing may be rendered less effective in strong winds due to its imbalance relative to the rotor diameter. On the other hand, a medium length fairing offers better results, as it maximizes power gains and performance generation. Finally, a long fairing assures optimum performance, but power losses can occur at high velocities.

In summary, when the fairing chord length is too short or too long, an unstable vortex field develops between the turbine and the fairing, particularly at the leading and trailing edges. This instability can increase torque and disrupt low-velocity flow. On the other hand, a chord length of average value favors the appearance of a more regular and stable flow zone. This suggests that optimal dimensioning of the fairing length not only improves flow behavior, but also significantly reduces the stagnation zone.

Vorticity contours reveal the formation of vortices when the blades are in motion, resulting in a turbulent regime in the areas around the rotor and fairing. These downstream-generated Kármán vortices (Palanisamy *et al.* 2019), which develop behind the blades in the form of a cylinder, have a crucial effect on the fluid dynamics around vertical-axis turbines, Comprehension of these phenomena is essential to optimize aerodynamic performance and improve turbine energy efficiency. In addition, a DAE-11 type fairing with medium chord lengths helps overcome the effect of turbulence by generating lift on the rotor, thus improving performance.

Figure 13 compares the total pressure distribution around the three-bladed H-Darrieus rotor with NACA0018 profile and equipped with different fairing types at α = 15°, for an optimum chord length of $C_{Fairing}$ = 3 and at different rotation angles θ. Based on the comparative study in Fig. 6, 7 and 8, we have selected a chord length of C = 0.850 for the NACA0018 profile of the H-Darrieus rotor, due to its enhanced performance. This prompted us to adopt this profile, which we endowed with three types of fairing. We then observed that the airfoil equipped with the DAE-11 fairing interacts with the rotor, presenting high pressure by producing vortex regions and moving external to the rotor towards the trailing edge, forming wake zones that are larger and more stable, meaning that the turbine faired by the DAE-11 airfoil operates efficiently under these conditions. On the other hand, this interaction plays an important role in optimizing and improving turbine performance. On the other hand, at θ = 45°, the blades are directly exposed to the airflow, and optimal lift is generated. At θ = 90°, the blades are perpendicular to the wind direction, which can result in airflow

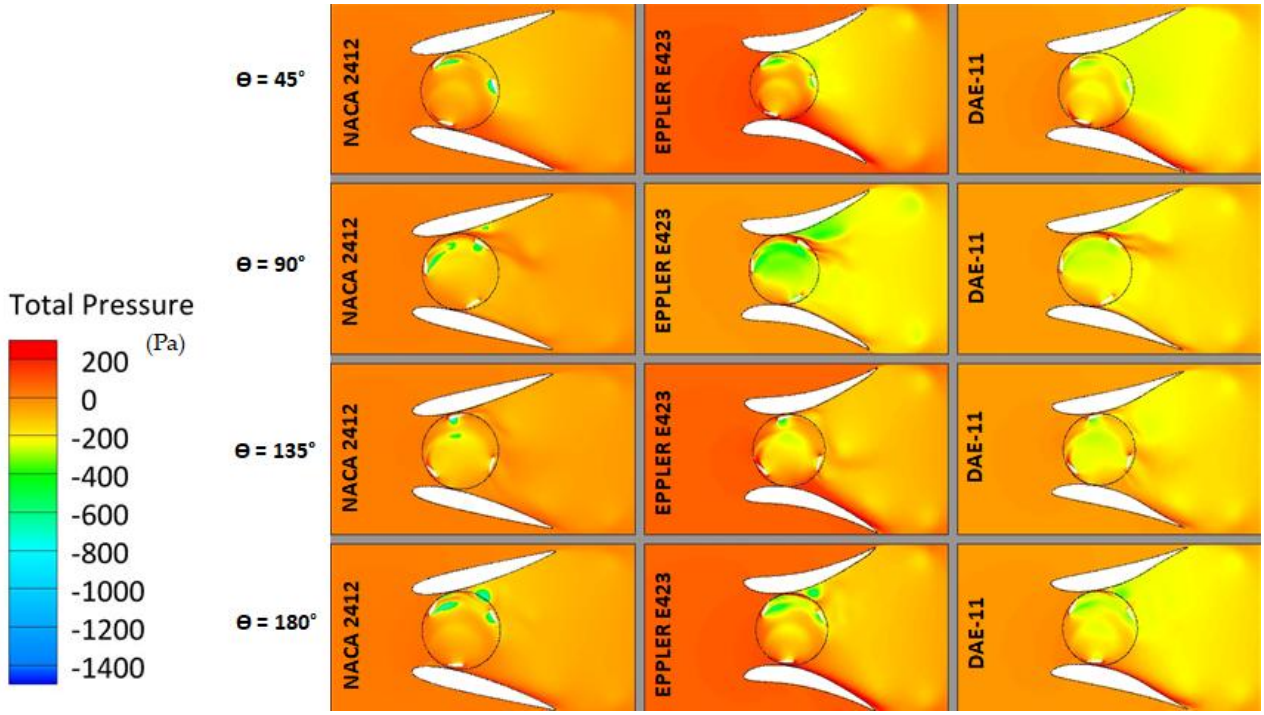

Fig.13 Total pressure distribution for the three fairing types for different rotation angles.

separation and energy loss. At θ = 135°, a good position is regained by the blades, leading to improved performance. At θ = 180°, the blades are positioned opposite to the wind direction, which has a significant impact on the aerodynamic forces (Fig. 13). Airflow may begin to separate from the surface, causing vortices to be formed behind the blades. These total pressure contours (Fig. 13) illustrate that the downstream vortex zones move outwards from the rotor to the trailing edge. However, the DAE-11 profile interacts with the rotor to generate wider, more stable wake zones for each position of the angle of rotation. It can be concluded that low total wake pressure indicates a reduction in wind velocity by the turbine. It's a sign of energy loss rather than improved performance.

The pressure field from the study of (Fertahi *et al.* 2023) shows that at different rotational positions, pressure varies regularly, with a stronger depression at position θ = 90° and a more balanced pressure at θ = 270°. Increasing the angle of attack causes an increase in pressure gradients, favoring lift but also potentially reinforcing flow separation. Several studies (Rohini *et al.* 2022; Ramesh *et al.* 2019) have been conducted to optimize the performance of the H-Darrieus rotor using the MRF method without fairing, aiming to improve the efficiency of the H-Darrieus turbine. However, based on the results and observations, integrating a fairing into the rotor led to a significant improvement in the turbine aerodynamic performance, particularly in terms of energy efficiency, flow stability, and reduced pressure losses. These improvements suggest that adding a fairing could play a key role in optimizing the performance of the H-Darrieus rotor by promoting more efficient flow. Moreover, it protects the mechanical components of the turbine from rain, ice, and helping to extend its lifespan and reduce maintenance costs.

5. Conclusion

This study delivered the improvement of the aerodynamic performance of the H-Darrieus vertical-axis turbine with three NACA0018 airfoil blades, using 2D CFD simulation based on solving the Steady Reynolds-Averaged Navier-Stokes equations (RANS) by applying the MRF method and the $k-\omega$ SST turbulence model. The validation of our simulation model was carried out for the H-Darrieus turbine without fairing, comparing the Sliding Mesh (SM) and Multiple Reference Frame (MRF) methods, based on the evolution of the power coefficient (C_P) as a function of the tip speed ratio (TSR). This comparison showed a good correspondence between our results and those obtained by (Balduzzi *et al.* 2016).

The results of our study show that optimal fairing design significantly improves turbine energy capture by effectively directing the flow around the blades. The main CFD results obtained are presented below:

- The DAE-11 fairing performs better than the Eppler 423 and NACA2412 profiles, particularly at higher angles of attack, and in particular in the power coefficient (C_P) which reaches the highest value of 0.607 for DAE-11 at C = 3, for TSR = 2.5 and at α = 0°, as well as in the C_m which reaches a maximum value of 0.354 for α = 20° on the DAE-11 fairing.
- Analysis of the flow field reveals that a short fairing can be considered less effective in strong winds. Furthermore, when the fairing is combined with a long chord, the complexity of the flow increases, which can also lead to a reduction in performance. On the other hand, a medium-length fairing seems to offer better results, maximizing power gains while limiting the undesirable effects of turbulence.
- The wind turbine equipped with the DAE-11 fairing interacts with the rotor, generating high pressure. This interaction generates vortex regions that propagate outwards from the rotor towards the trailing edge, contributing to the formation of stable wake zones.

In conclusion, observations show that the integration of an optimal type of fairing to the H-Darrieus rotor led to a significant improvement in the aerodynamic performance of the turbine,

particularly in terms of flow stabilization and reduced pressure losses. These improvements suggest that the addition of a fairing could play a key role in optimizing the blade's angle of attack and enhancing the overall efficiency of the device by promoting more efficient flow. Furthermore, it protects the turbine mechanical components from rain and dust, there by contributing to a longer lifespan and reduced maintenance costs. Future work will include the analysis of 3D flow effects to optimize the design of small and large H-Darrieus turbines.

Acknowledgments

The authors would like to take this opportunity to sincerely thank the editor and reviewers for their prompt review and valuable comments, which have considerably improved the quality of this scientific contribution.

Author Contribution: The authors confirmed the contribution to this article as follows: D. Boulla: Conceptualization, Methodology, Validation, Investigation, Resources, Writing—Original Draft, Software, Visualization, Formal analysis, Writing—Review and Editing, S. Fertahi: Methodology, Software, Validation, Investigation, Resources, Writing, Funding Acquisition, Supervision and Visualization, M. Bernatchou: Methodology, Validation, Investigation, Resources, Writing, Supervision and Visualization, A. Samaouali, M. Ajani, Ch. Boussaq: Supervision, Validation, Investigation and Visualization. The manuscript was written through the contribution of all authors. All authors discussed the results, reviewed, and approved the final version of the manuscript.

Funding: The authors received no financial support for the research, authorship, and publication of this article.

Conflict of Interest: The authors declared no potential conflicts of interest concerning the research, authorship, and publication of this article.

References

Ahmad, M., Shahzad, A., Akram, F., Ahmad, F., Shah, S.I.A. (2022). Design optimization of Double-Darrieus hybrid vertical axis wind turbine, *Ocean Eng.*, 254, 111171; https://doi.org/10.1016/j.oceaneng.2022.111171

ANSYS Inc, (2014). Introduction to Ansys Fluent-Turbulence Modeling.; https://doi.org/10.1016/j.prime.2023.100178

Asr, M.T., Nezhad, E.Z., Mustapha, F., Wiriadidjaja, S. (2016). Study on start-up characteristics of H-Darrieus vertical axis wind turbines comprising NACA 4-digit series blade airfoils, *Energy*, 112, 528e37; https://doi.org/10.1016/j.energy.2016.06.059

Balduzzi, F. Bianchini, A. Maleci, R. Ferrara, G. Ferrari, L. (2016). Critical issues in the CFD simulation of Darrieus wind turbines, Renew Energy January, 85: 419e35; http://dx.doi.org/10.1016/j.renene.2015.06.048.

Bausas, M.D., Danao, L.A.M. (2015). The aerodynamics of a camberbladed vertical axis wind turbine in unsteady wind, *Energy*, 93, 1155e64; https://doi.org/10.1016/j.energy.2015.09.120

Castelli, R., Englaro, A., Benini, E.(2011) The Darrieus wind turbine: proposal for a new performance prediction model based on CFD, *Energy*, 36, 4919–4934; https://doi.org/10.1016/j.energy.2011.05.036

Celik, Y., Ma, L., Ingham, D., Pourkashanian, M. (2020). Aerodynamic investigation of the start-up process of H-type vertical axis wind turbines using CFD, J. *Wind. Eng. Ind. Aerodyn*, 204, 104252. https://doi.org/10.1016/j.jweia.2020.104252

Chandra, S., Tyagi, R. (2020). Study of Eppler 423 Airfoil with Gurney

Chowdhury, N.E., Shakib, M.A., Xu, F., Salehin, S., Islam, M.R., Bhuiyan,A.A (2022). Adverse environmental impacts of wind farm installations and alternative research pathways to their mitigation, *Clean Eng Technol*, 7, 100415; https://doi.org/10.1016/j.clet.2022.100415

Chunyan, Z., Shuaishuai, W., Yinhu, Q., Zhiqiang, Z. (2023). Optimized Design of H-Type Vertical Axis Wind Airfoil at Multiple Angles of Attack, *Fluid Dynamics & Materials Processing*, 19, 10; https://doi.org/10.32604/fdmp.2023.028059

Douha, B., Saïf ed-Dîn, F., Maryam, B., Abderrahim, S. (2025). CFDNumerical Simulation Study of Aerodynamic Performance of H Darrieus Rotor, CFD Letters, 17, 6, 117; https://doi.org/10.37934/cfdl.17.6.117

Flap and Vortex Generators, *Advances in Aerospace Science and Technology*, 05, 51001; https://doi.org/10.4236/aast.2020.51001

Fluent, A. (2020). Ansys fluent theory guide. ANSYS Inc., USA, pp. 00011026. URL https://www.ansys.com/

Fluent, A. N. S. Y. S. (2011). Ansys fluent theory guide. Ansys Inc., USA, 15317, 724-746; URL https://www.ansys.com/

Gebreel, A.,William, M., Fue-Sang, L. (2017). Pitch angle control for a small-scale Darrieus vertical axis wind turbine with straight blades (H-Type VAWT), *Renewable Energy*, 114, 1353e1362; https://doi.org/10.1016/j.renene.2017.07.068

Gemayel, D., Abdelwahab, M., Ghazal, T., Aboshosha, H. (2023). Modelling of vertical axis wind turbine using large eddy simulations, *Results in Engineering*, 18, 101226; https://doi.org/10.1016/j.rineng.2023.101226

Hau E. (2006) Wind turbines: fundamentals, technologies, application, economics. Publisher: Berlin, Springer-Verlag.

Hoseinzadeh, S., Amin, B., Seyed, M.M., Ali, S., Stephan, H. (2020). A detailed experimental airfoil performance investigation using an equipped wind tunnel, *Flow Measurement and Instrumentation*, 72, 101717; https://doi.org/10.1016/j.flowmeasinst.2020.101717

Ian Carlo, M.L, Louis, A.M.D. (2019) Steady wind performance of a 5 kW three bladed H-rotor Darrieus Vertical Axis Wind Turbine (VAWT) with cambered tubercle leading edge (TLE) blades, *Energy,* 175, 278-291; https://doi.org/10.1016/j.energy.2019.03.033

Inc, A. ANSYS fluent (2020) R1, user's guide, 11.6.5. Six DOF solver settings, 11.6.5.1. Setting rigid body motion attributes for the six DOF solver. 2020; URL https://www.ansys.com/

Kanyako, F., Janajreh, I. (2015). Vertical axis wind turbine performance prediction models using high and low fidelity analyses, *Int J Eng Res Innovation*, 7, 48e56; https://doi.org/10.1109/InnoTek.2014.6877366

Kevin, R., Moore, B.L.E. (2020). Vertical-Axis Wind Turbine Steady and Unsteady Aerodynamics for Curved Deforming Blades, *SAND*, 87185; https://doi.org/10.15632/jtam-pl.56.1.203

Krzysztof, R., Martin, O.L.H., Galih, B. (2020). Performance Analysis of a H-Darrieus Wind Turbine for a Series of 4-Digit NACA Airfoils, *Energies*, 13, 3196; https://doi.org/10.3390/en13123196

Maalouly, M., Souaiby, M., ElCheikh, A., Issa, j.s, Elkhoury, M. (2022). Transient analysis of H- type Vertical Axis Wind Turbines using CFD, *Energy Reports*, 8, 4570–4588; https://doi.org/10.1016/j.egyr.2022.03.136

Mahdi, T.A., Erfan, Z.N., Faizal, M., Surjatin, W. (2016). Study on start-up characteristics of H-Darrieus vertical axis wind turbines comprising NACA 4-digit series blade airfoils, *Energy*, 112, 528e537; https://doi.org/10.1016/j.energy.2016.06.059

Maître, T., Amet, E., Pellone, C., Modeling of the flow in a Darrieus water turbine: Wall grid refinement analysis and comparison with experiments. *Renewable Energy*, 51, 497-512; https://doi.org/10.1016/j.renene.2012.09.030

Mandar, T., Salman, M.S., Adil, R., Trond, K. (2017). Scale turbine and associated wake development -comparison of RANS based Actuator Line Vs Sliding Mesh Interface Vs Multiple Reference Frame method, *Energy Procedia*, 137, 477–48;

Marini, M., Aristide, M., Antonio, S. (1992). Performance of vertical axis wind turbines with different shapes, *Journal of wind engineering and industrial aerodynamics*, 39, 1-3 83-93; https://doi.org/10.1016/0167-6105(92)90535-I

Menter, F.R. (1994). Two-equation eddy-viscosity turbulence models For engineering applications. *AIAA J*, 32, 8 1598–605; https://doi.org/doi.org/10.2514/3.12149

Milad, Y.R., Khaleghini, j., Majid, E.N. Hesamoddin, S. (2021). Performance improvement of Darrieus wind turbine using different cavity layout, *Energy Conversion and Management*, 246, 114693; https://doi.org/10.1016/j.enconman.2021.114693

Mohammed, S., Shaaban, A. (2017). à Efficient clusters and patterned farms for Darrieus wind turbines, *Sustainable Energy Technologies and Assessments*, 19, 125-135; https://doi.org/10.1016/j.seta.2017.01.007

NEA Releases National Power Industry Statistics (2022). Available online: https://www.nea.gov.cn/2023-01/18/c_1310691509.htm (accessed on 12 October 2024).

Palanisamy, M.K,Mohan, R.S., Krishnamoorthi, S., Teik, C.L., Seeram, R., He, W. (2019). Computational Optimization of Adaptive Hybrid Darrieus Turbine: Part 1, *Fluids*, 4(2), 90; https://doi.org/10.3390/fluids4020090

Paulo, A.S.F., Silva, P., Tsoutsanis, A., Antoniadis, F. (2021). Simple multiple reference frame for high-order solution of hovering rotors with and without ground effect, *Aerospace Science and Technology*, 111, 10651; https://doi.org/10.1016/j.ast.2021.106518

Pedram, G., Gholamhassan, N., Barat, G., Ali. J., Rizalman, M., Mohd, F.G. (2023). CFD-Study of the H-Rotor Darrius wind turbine performance in Drag-Lift and lift Regime: Impact of Type, thickness and chord length of blades, *Alexandria Engineering Journal*, 67, 51-64; https://doi.org/10.1016/j.aej.2022.10.013

Peter, G., Raja, S., Axial, Fan. (2011). Performance Predictions in CFD, Comparison of MRF and Sliding Mesh with Experiments, *SAE Technical Paper*, 01, 0652; https://doi.org/10.4271/2011-01-0652

Qamar, S.B., Janajreh, I. (2017). Investigation of effect of cambered blades on Darrieus VAWTs, *Energy Procedia*, 105, 537e43; https://doi.org/10.1016/j.egypro.2017.03.353

Qasemi, K., Azadani, L.N. (2020). Optimization of the power output of a vertical axis wind turbine augmented with a flat plate deflector, *Energy*, 202, 117745; https://doi.org/10.1016/j.energy.2020.117745

Ramesh, M., Vijayanandh, R., Acoustic Investigation on Unmanned Aerial Vehicle's Rotor Using CFD-MRF Approach, Gas Turbine India, 2019, 7, 2430; https://doi.org/10.1115/GTINDIA2019-2430

Rogowski, K., Hansen, M.O.L., Maronski, R. (2018). Steady and Unsteady Analysis of NACA0018 Airfoil in Vertical-Axis Wind Turbine. *Journal of Theoretical and Applied Mechanics*, 56, 203-212;

Rohini, J.B., Hussein, A.Z., AL-bonsrulah, V.R., Lokeshkumar, K., Sri Diviyalakshmi, K., Senthil, K.M., Raffik, R., Parvathy, R., Mohammed, A.l.B. (2022). Design and multiperspectivity-based performance investigations of H-Darrieus vertical axis wind turbine through computational fluid dynamics adopted with moving reference frame approaches, *International Journal of Low-Carbon Technologies*, 17, 784–806; https://doi.org/10.1051/epjconf/20159202058

Rosario, L., Stefano, M., Michele, M., Sebastian, B. (2020). Development and Validation of CFD 2D Models for the Simulation of Micro H-Darrieus Turbines Subjected to High Boundary Layer Instabilities, *Energies*, 13, 5564; https://doi.org/10.3390/en13215564

Saïf ed-Dîn, F., Samaouali, A., Kadiri, I. (2023). CFD comparison of 2D And 3D aerodynamics in H-Darrieus prototype wake, E-Prime Advances in Electrical Engineering, *Electronics and Energy*, 4, 100178;

Saïf ed-Dîn, F., Tarik, B., Anass, K., Abderrahim, S., Imad, K. (2023).Assessment of fairing geometry effects on H-Darrieus hydro turbine performance using 2D URANS CFD simulations. *Energy Conversion and Management*, 293, 117434; https://doi.org/10.1016/j.enconman.2023.117434

Sedaghat, A., Hassanzadeh, A., Jamali, J., Mostafaeipour, A., Chen, W.H. (2017). Determination of rated wind speed for maximum annual energy production of variable speed wind turbines. Appl. *Energy*, 205, 781–789; https://doi.org/10.1016/j.apenergy.2017.08.079

SWei, H.C., Trinh, T.L., Min, H.C., Liwen, J., Chih, C.C.h., Gerardo, L.A. (2024). Optimizing H-Darrieus Wind Turbine Performance with Double-Deflector Design, *Energies*, 17, 503; https://doi.org/10.3390/en17020503

Vennell, R. (2013). Exceeding the betz limit with tidal turbines, *Renew Energy*, 55, 277–85; https://doi.org/10.1016/j.renene.2012.12.016

Versteeg, H.K., Malalasekera, W. (2007). An introduction to computational fluid dynamics: The finite volume method, Pearson education; URL https://www.pearsoned.co.uk/versteeg

Wang, S., Ingham, D.B., Lin, M.a., Pourkashanian, M., Tao, Z. (2012). Turbulence modeling of deep dynamic stall at relatively low Reynolds number, *J Fluids Struct*, 33, 191e209; https://doi.org/10.1016/j.jfluidstructs.2012.04.011

Willmott, C.J., Ackleson, S.G., Davis, R.E., Feddema, J.J., Klink, K.M., Legates, D.R., O'donnell, J., Rowe, C.M. (1985). Statistics for the evaluation and comparison of models, *Oceans*, 90, C5 8995-9005; https://doi.org/10.1029/JC090iC05p08995

Ying, W., Sheng, S., Gaohui, L.i., Diangui, H., Zhongquan, Z. (2018). Investigation on aerodynamic performance of vertical axis wind turbine with different series airfoil shapes, Renewable Energy, 126, 801-818;https://doi.org/10.1016/j.renene.2018.02.095

Zhandos, B., Taeseong, K., Chankyu, S. (2021). Numerical method to predict ice accretion shapes and performance penalties for rotating vertical axis wind turbines under icing conditions, *Journal of Wind Engineering and Industrial Aerodynamics*, 216, 104708; https://doi.org/10.1016/j.jweia.2021.104708

Zhao, Z., Wang, D., Wang, T., Shen, W., Liu, H., Chen, M., A review: Approaches for aerodynamic performance improvement of lift-type vertical axis wind turbine, Sustain. *Energy Technol. Assess.*, 49, 101789;